DOI: 10.1142/S2424905X1640002X

Journal of Medical Robotics Research, Vol. 0, No. 0 (2015) 1–11

Ultrasound-based Image Guidance and Motion Compensating Control for Robot-assisted Beating-heart Surgery

Meaghan Bowthorpe, Mahdi Tavakoli

Department of Electrical and Computer Engineering, University of Alberta, Edmonton, AB, T6G 2V4, Canada
E-mail: meaghan.bowthorpe@ualberta.ca, mahdi.tavakoli@ualberta.ca

Performing a surgical task on a beating heart requires superhuman skill as the surgeon must manually track the heart's motion while performing a surgical task. However, the ability to operate on a beating heart would eliminate the need to use a mechanical stabilizer or arrest the heart and connect the patient to a heart-lung machine and would consequently eliminate their side effects. This work develops the image processing and control structure for an ultrasound-guided robot-assisted beating heart surgical system that will move the surgical tool tip in synchrony with the heart. This would allow the surgeon to operate through teleoperation on a virtually stabilized point on the heart. In developing this system, the position data acquired from ultrasound images is upsampled and predicted ahead to compensate for the image acquisition and processing delay. We present the results of a user task based on mitral valve annuloplasty performed under ultrasound guidance.

Keywords: Ultrasound Guidance; Robot-assisted Surgery; Teleoperation.

Nomenclature

EKF	Extended Kalman filter
POI	Point of interest
ROI	Region of interest
${}^{I}X$	Position measurement X in the image frame
${}^{R}X$	Position measurement X in the robot frame
$\bar{X}$	Time delayed value of X
$\hat{X}$	Estimated value of X
X'	Slowly sampled discrete value of X
X''	Fast sampled discrete value of X
D	Distance between the surgical tool tip and the POI
P_{POI}	Position of the POI
P_S	Position of the surgeon
P_T	Position of the surgical tool tip

1. Introduction

The ability to operate on a freely beating heart offers many benefits to patients. Currently, if a surgical procedure is performed on a beating heart, a mechanical stabilizer is used to locally suppress the beating motion. However, mechanical stabilizers fail to eliminate all of the heart's beating motion and can damage the heart's tissue.[1] For complex procedures or ones performed inside the heart, the patient's heart is currently arrested and a heart-lung bypass machine circulates the patient's blood and ventilates the lungs. However, this increases the patient's risk of stroke and can cause long-term cognitive loss.[2,3]

To date, performing a surgical procedure on a freely beating heart remains nearly impossible as the surgeon must manually compensate for the heart's beating motion while performing the surgical procedure. However, the ability to operate on a beating heart has the potential to improve the outcome of surgical procedures. For example, more than 300,000 people undergo mitral valve annuloplasty each year worldwide.[4] If securing this annuloplasty ring could be performed while the heart is still beating, the effectiveness of the newly reshaped valve could be evaluated immediately, which is not currently possible. The use of robotic assistance has the potential to greatly reduce the disturbing effects of heartbeat-induced motion during interventions. By controlling a surgical robot to move in synchrony with the point of interest (POI) on the beating heart, the POI can be made stationary with respect to the surgical robot's tool tip. Then, the surgeon could operate on a seemingly stationary heart via teleoperation. This will allow for safer, more effective interventions that can be evaluated on the fly in the operating room as the heart will continue beating throughout the procedure.

2. Prior Art

To provide meaningful assistance, the surgical robotic system must compensate for the physiological motion. *The goal of the physiological motion compensation is to make*

the surgical tool tip follow the combination of the POI's and the surgeon's motion. Depending on the desired cardiac surgical procedure, the design of the robot-assisted beating heart surgical system will vary. However, certain components are common to all designs: a method of measuring the positions of the surgical tool tip and the POI on the heart, and a controller that moves the surgical tool tip in synchrony with the POI on the heart and then superimposes the surgeon's motion.

2.1. *Control System Configuration*

The POI motion measurement methods can be divided into two categories: (a) position sensors such as sonomicrometry crystals, and (b) image-based sensors, which includes cameras, endoscopes, and ultrasound imaging. The control system maintains a desired distance between the surgical tool tip and the heart tissue.

An alternative that does not require the surgical tool tip and the heart to remain in contact is to maintain a desired distance. In this scenario, the surgical tool tip will follow the motion of the heart tissue whether or not it is in contact with the heart tissue. Some methods first reduce the heart's physiological motion using a mechanical stabilizer; however, they are only useful for procedures on the outside of the heart and still can cause damage to the heart tissue.[1]

Other proposed methods allow the heart to beat freely.[5–14] To maintain a desired distance, the position of the heart tissue must be measured. One method is to use sonomicrometry crystals that are sutured to the heart tissue (case (a)).[5–9] Improved algorithms have reduced the data processing time in [9], but this method still cannot be used in real-time. Alternatively, different types of images can be used (case (b)). For example, a 955 Hz camera is used for coronary artery bypass graft.[10] Later, a slower camera with a frame rate of 500 Hz and compensation for the one sample time of image processing delay is presented in [11, 12]. However, high-speed cameras and endoscopes can only visualize the outer surface of the heart and, therefore, are not feasible for procedures performed inside the heart such as valve repairs.

To visualize the interior of the heart through the opaque blood pool, medical images are needed. MRI or CT are expensive, difficult to have in an operating suite, and are not real-time modalities. Ultrasound images are more appropriate even though they have a slow frame rate, typically in the range of 20 to 60 Hz. This issue is compounded by the large ultrasound image acquisition delay and the subsequent image processing delay.

2.2. *Surgical Tool Configuration*

Previously, a hand-held surgical tool has been developed by Kettler et al. for mitral valve repair.[15] Processing the ultrasound image of the heart and surgical tool and subsequently servoing the tool in real-time based on the position data was developed by Novotny et al. in [16] and [17], respectively. Finally, the control system that moved this hand-held tool in synchrony with the mitral valve was developed by Yuen et al.[14] A limitation of the hand-held tool approach is that if the hand-held surgical tool comes into contact with the heart, it is difficult to determine where the tool tip is.

The use of a hand-held tool does not take advantage of the benefits of teleoperated robotic surgery where the surgeon operates from a separate user console with a more ergonomic posture. In addition, teleoperation can enhance the surgeon's performance as the surgeon's motions can be scaled and hand tremors can be reduced.[18] With teleoperated tools, the position of the surgical tool can easily be recorded, which is much more difficult with hand-held tools. Having this trajectory data is important for skill assessment as the motion trajectories of experienced and non-experienced surgeons can be compared as they complete the same task.[19]It is also important for enhanced documentation and the development of surgical simulation systems. Teleoperation is also important for training new surgeons as trilateral teleoperation systems allow experienced and non-experienced surgeons to operate a single slave robot (the surgical robot) together.[20] In the teleoperation mode, control of the surgical robot can also be split between between a control system and a surgeon if, for example, the surgical tool should not cross into a specific area. This split control could also maintain a desired contact force between an ultrasound probe and the patient, while the physician controls the other degrees of freedom of the probe's position to find the desired imaging plane.[21]

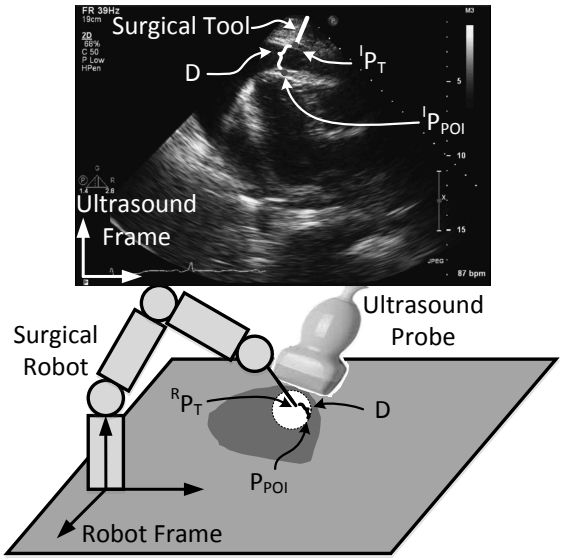

Fig. 1. The position of the surgical tool tip and the POI on the heart are measured in the ultrasound frame. The position of the surgical tool tip is measured in the robot frame.

Previously, we proposed a teleoperated robotic surgical system in [22], where a Smith predictor maintained the stability of the system despite the time delays. The time delays were introduced by a Micron Tracker used to measure the position of the surgical tool and the POI from images using its own software. In this paper, ultrasound images are used to measure the position of the POI and a detailed description of the required image processing is included. Also, [22] only tested the surgical tool's ability to synchronize with the POI's motion when the surgeon's motion was a preset trajectory that did not make the surgical tool come into contact with the POI. The image processing presented in this paper; however is developed such that motion tracking continues even when the surgical tool is in contact with the heart tissue and it is hard to differentiate the two in the ultrasound images. Previously, no user trials were performed in [22]. In this paper we conduct a user study on a task based on mitral valve annuloplasty under ultrasound guidance with a teleoperated motion-compensating beating-heart surgical robot.

This paper is organized as follows. The development of the robot-assisted surgical system is presented in Sec. 3. The image processing algorithm that finds the surgical tool tip and the POI in each ultrasound image is outlined in Sec 3.2. The POI's slowly sampled motion is then upsampled in Sec. 3.3. Finally, to compensate for the delays, the POI's motion is predicted ahead to the current time in Sec. 3.4. The experimental setup is described in Sec. 4 and the surgical task based on mitral valve annuloplasty is described in Sec. 4.1. The conclusion is presented in Sec. 5.

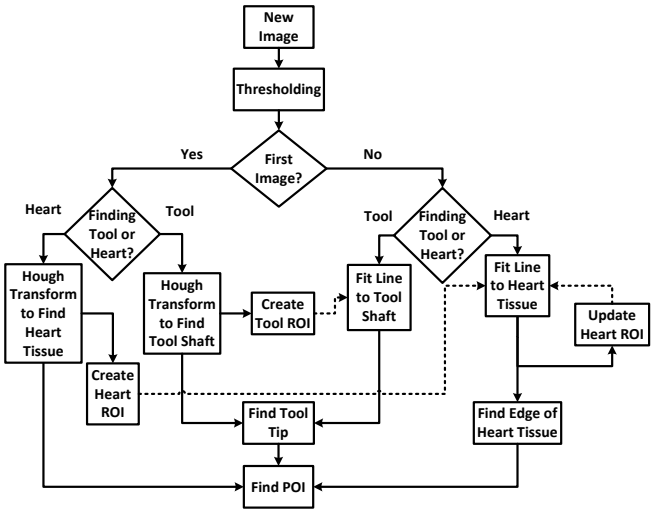

Fig. 2. A flow chart of the image processing. Each image is thresholded to create a black and white image. Hough transforms are then used to locate the tool shaft and heart tissue in the first image. The ROIs are set and the tool tip and POI locations are found. Lines are then fit to the tool shaft and heart tissue in the remaining images, the edge of the heart tissue is found, the heart tissue ROI is updated, and the tool tip and POI locations are found.

3. System Development

The feedback control structure synchronizes the distance between the surgical tool tip and the POI. When designing this controller, either the controller itself must compensate for the delayed position measurements, or the delayed position measurements must be predicted forward to the current time before being fed to the controller. Previously, we took the former approach in [22] and [23]. In this work, a simpler controller will be used and the delayed position measurements are predicted forward to the current time.

3.1. *Predictive Feedback Control of the Surgical Robot*

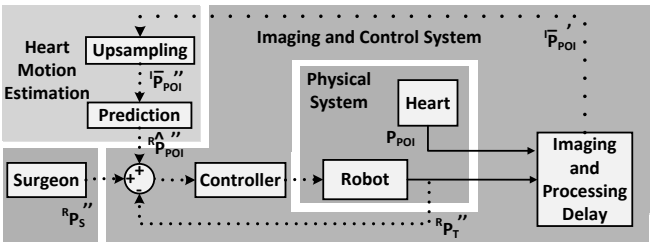

Fig. 3. A simple feedback controller for teleoperated motion compensation. Here, the setpoint for the robot's position, ${}^{R}P_{T}''$ is the combination of the surgeon's position, ${}^{R}P_{S}''$, and the estimated current POI position ${}^{R}\hat{P}_{POI}''$.

A diagram of the utilized feedback loop is given in Fig. 3. The surgical tool tip's motion will be controlled to follow the combination of the estimated POI's motion and the surgeon's motion. First, the POI's motion is upsampled according to (1) as described below in Sec. 3.3, predicted ahead according to (3a and 8) as described below in Sec. 3.4, and converted into the robot's frame of reference to become ${}^{R}\hat{P}_{POI}''$.

3.2. *Ultrasound Imaging*

To design a control system that will make the surgical tool tip follow the combined surgeon's and POI's motion, the surgeon's and the POI's motion must be measured. The surgical robot's position and hence the position of the surgical tool tip can be measured in the robot's frame of reference without a delay at a fast sampling rate from the surgical robot's encoders and is denoted ${}^{R}P_{T}''$. The surgeon's motion can also be measured at this high sampling rate without any delay from the user console and is denoted ${}^{R}P_{S}''$. As the surgeon's motion is assumed to be one-dimensional, the distance between the surgeon's hand position and the user console's zero position is the same distance the slave robot should move and hence, this measurement is considered to be in the robot's frame of reference. The POI's motion is measured in ultrasound images that are acquired at a slow

sampling rate. The images need to be processed to find the location of the POI which means the measurements will be delayed and the POI's position is denoted ${}^{I}\bar{P}'_{POI}$.

For the proposed robot-assisted beating heart surgical system to perform procedures on the interior surface of the heart as well as the exterior surface, the imaging modality must be able to visualize the heart tissue through the opaque blood pool. For this reason, medical images were chosen despite the slow image acquisition rate. Ultrasound imaging is the most portable and least expensive medical imaging modality and hence, was chosen for this work. The purpose of the imaging is to locate the surgical tool and the POI, which is the point on the heart tissue the surgical tool is pointing directly towards. These position measurements will be found in the image frame as shown in Fig. 1.

The image processing method presented in this paper does not require the use of any markers and is completed within one sample time of the image acquisition rate of 34 Hz. The image processing begins by applying a binary threshold to convert the gray-scale images to black and white images. The remaining processing is based on finding lines in the images as the shaft of the surgical tool is a straight rod. The image processing procedure is summarized in Fig. 2.

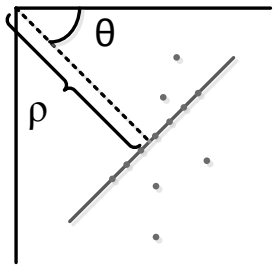

Fig. 4. A Hough transform converts all points in the image to polar coordinates. All points on a single line share the same ρ and θ value.

The surgical tool, which has the shape of a long straight line, is found first in each image. In the first image, this is done using a Hough transform. The Hough transform converts the rectangular coordinates of each white point in the image into polar coordinates and a line is characterized by the perpendicular distance between the line and the origin (ρ) and the angle that ρ makes with respect to the horizontal (θ), as shown in Fig. 4. All of the points on a single line have the same ρ and θ values. A ρ and θ pair is considered to represent a line if enough points in the image have been converted into this pair in polar coordinates. To find the correct line (as there will be multiple lines in the image), only a range of $\frac{\pi}{4}$ θ values surrounding where the surgical tool is expected to be is analyzed. The longest line found in this region is the surgical tool shaft. Throughout the procedure, the surgical tool is confined to one-dimensional motion. To reduce the processing time of the remaining images, a region of interest (ROI) is created in the area surrounding the determined location of the surgical tool and is set as the region of interest.

The Hough transform is a computationally expensive method of finding lines. In addition, as the tool shaft is a thick line, the longest line found by the Hough transform is not necessarily the centre line and may not be parallel with the tool shaft (e.g., the longest line may begin in the upper right corner of the tool and end in the lower left corner). To correctly identify the centre line of the tool shaft least squares regression is used in the remaining images, which minimizes the distance between the line and all of the candidate pixels. To minimize the computation time when identifying the candidate pixels contained within the ROI, the image is down-sampled and only every third column and third row are analysed. A line is then fit through these points using OpenCV's fitline().[24] Once the tool's shaft has been identified, the surgical tool tip, ${}^{I}\bar{P}'_{T}$, is found by extending the line along the surgical tool shaft until the last candidate pixel point. Fig. 5 shows the result of finding the tool. The ROI surrounding the tool shaft is marked by the green lines, the center of the tool shaft is given by the purple line, and the tool tip is shown my the blue dot.

Fig. 5. The result of the image processing required to find the surgical tool shaft and tip. The green lines form the boundary of the ROI, the purple line identifies the surgical tool shaft, and the blue dot shows the surgical tool tip.

The heart tissue is found in a manner similar to the tool's shaft. In the first image, a Hough transform identifies the longest line within a $\frac{\pi}{4}$ range of θ values perpendicular to the surgical tool shaft. A new ROI is then created to identify the area surrounding the heart tissue. In all subsequent images, the heart tissue is identified by fitting a line using least squares regression. Once again, to minimize the computation time when identifying the candidate pixels contained within the ROI, the image is down-sampled and only every third column and third row are analysed. Within every subsequent image, the candidate pixels on the upper edge of the heart tissue are identified and a straight line is fit through them. As the heart tissue moves continually, the ROI surrounding the heart tissue is updated after every image. Fig. 6 shows the result of finding the heart

tissue. The ROI surrounding the heart tissue is marked by the light green lines, the edge of the heart tissue is given by the dark green line, and the centre line of the heart is given by the red line.

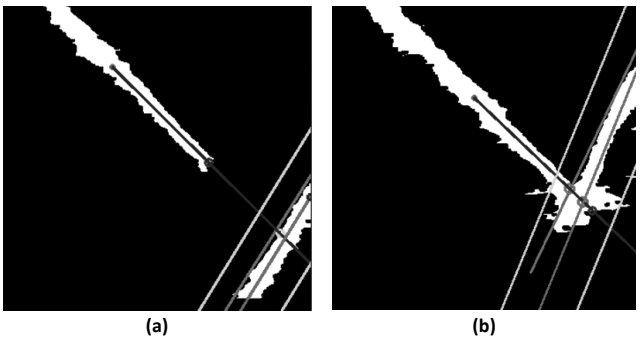

Fig. 6. The result of the image processing required to find the heart tissue and POI. The light green lines form the boundary of the ROI, the red line identifies the heart tissue, and the dark green line identifies the edge of the heart tissue. When the surgical tool does not touch the heart in (a) the green dot identifies the location of the POI, and when the surgical tool touches the heart in (b) the pink dot identifies the location of the POI

The goal of the motion compensating controller is to maintain a desired distance between the tip of the surgical tool and the POI. Since the POI location is reported with a slow sampling rate (ultrasound image refresh rate) and is subject to the image acquisition and processing delays, it is denoted ${}^I\bar{P}'_{POI}$. The location of the POI is found by extending the line through the surgical tool shaft and locating the first candidate pixel beyond the surgical tool's tip – the heart tissue. However, a difficulty arises when the surgical tool tip makes contact with the heart tissue. In this case, it is still possible to identify the shaft of the surgical tool, but not its tip location nor the location of the POI as the surgical tool and the heart tissue will appear as one solid object in the image. To separate the two, we begin by determining whether the surgical tool tip has collided with the heart. If the line identifying the tool shaft intersects with the line through the heart, there is a collision between the surgical tool tip and the heart tissue. In this scenario, the POI is identified by the intersection of the line found along the edge of the heart tissue and the line through the surgical tool shaft. Fig. 6 shows the location of the POI when the surgical tool and the heart do not touch – green dot in (a) – and when they do – pink dot in (b).

There are two main challenges to overcome when using ultrasound guidance: the slowly sampled data and the image acquisition and processing delay. To overcome these challenges, we propose to first upsample the position data using cubic interpolation based upsampling. Next the POI's motion is predicted ahead for the duration of the image acquisition and processing delay to the current time using an extended Kalman filter (EKF).

3.3. *Heart Motion Data Upsampling*

To take advantage of the robot's faster sampling rate, the slowly sampled POI position data will be upsampled using cubic interpolation to 100 Hz. Cubic interpolation was chosen because it upsamples the motion in a smooth fashion and is robust.

The following equation describes the cubic interpolated upsampled data points $p(i)$:

$$p(i) = h_{00}(i)p_0 + h_{10}(i)m_0 + h_{01}(i)p_1 + h_{11}(i)m_1 \quad (1)$$

where the h coefficients are as follows:

$$h_{00}(i) = 2i^3 - 3i^2 + 1 \quad (2a)$$

$$h_{10}(i) = i^3 - 2i^2 + i \quad (2b)$$

$$h_{01}(i) = -2i^3 + 3i^2 \quad (2c)$$

$$h_{11}(i) = i^3 - i^2 \quad (2d)$$

and p_0 and p_1 are the points in between which the interpolation is occurring, and m_0 and m_1 are the slopes at p_0 and p_1, respectively. The interpolation variable i contains evenly spaced values between 0 and 1, and has a length of one greater than the number of points to be upsampled between the two slowly sampled points p_0 and p_1. As four data points are required (points p_0 and p_1 and a data point on either side used to calculate the slope) to ensure that the upsampled signal and its first derivative are continuous, cubic interpolation involves a processing delay of $2n-1$ fast sample times, where n is the number of samples added to the signal. The POI's motion, ${}^I\bar{P}''_{POI}$ is now estimated at the fast sampling rate, but it is still delayed.

3.4. *Heart Motion Data Prediction*

Once the position data has been upsampled, the POI's position must be predicted ahead to the current time to overcome the image acquisition and processing delay inherent in ultrasound-based POI motion tracking as well as the delay caused by cubic interpolation, which is 170 ms. Here an EKF is used for prediction as it allows for a changing heart rate and changing amplitude in the motion signal.

The signal model $y(\mathbf{x}(t))$ for the POI's position is a Fourier series in which the coefficients can vary with time (3):[14,25]

$$y(\mathbf{x}(t)) \triangleq c + \sum_{l=1}^{m} r_l \sin\theta_l(t) \quad (3a)$$

$$\theta_l(t) = l\int_0^t \omega(\tau)d\tau + \phi_l(t) \quad (3b)$$

$$\mathbf{x}(t) = [c(t), r_l(t), \omega(t), \theta_l(t)]^T \quad (3c)$$

The EKF describing the POI's motion is based on the state space model (4) that evolves through random walk, where the offset c, the sine wave coefficients r_l, and the frequency ω remain constant between samples. Only the θ_l values are updated according to (3b) each sample time.

These values are later updated by the EKF based on the error between the predicted and actual measurement.

$$\mathbf{x}(t+\Delta t) = \mathbf{F}(\Delta t)\mathbf{x}(t) + \mu(t) \tag{4a}$$
$$z(t) = y(\mathbf{x}(t)) + \upsilon(t) \tag{4b}$$

where

$$\mathbf{F}(\Delta t) = \left[\begin{array}{c|ccccc} \mathbf{I}_{m+1} & & & \mathbf{0} & & \\ \hline & 1 & & & & \\ & \Delta t & 1 & & & \\ \mathbf{0} & 2\Delta t & 0 & 1 & & \\ & \vdots & & & \ddots & \\ & m\Delta t & & & & 1 \end{array}\right]_{[2m+2]\times[2m+2]} \tag{5}$$

and $\mu(t)$ and $\upsilon(t)$ are independent Gaussian noise terms.

Next, the EKF is updated at the fast sampling rate by the following equations as the POI motion was previously upsampled from the slow sampling rate:

$$\mathbf{P}(t+\Delta t|t) = \mathbf{F}(\Delta t)\mathbf{P}(t|t)\mathbf{F}(\Delta t)^T + \mathbf{Q} \tag{6a}$$
$$S = \sigma_R^2 + \mathbf{H}(\Delta t)\mathbf{P}(t+\Delta t|t)\mathbf{H}(\Delta t)^T \tag{6b}$$
$$\mathbf{K}(t) = \mathbf{P}(t+\Delta t|t)\mathbf{H}(\Delta t)^T S^{-1} \tag{6c}$$
$$\hat{\mathbf{x}}(t+\Delta t|t+\Delta t) = \mathbf{F}(\Delta t)\hat{\mathbf{x}}(t|t) \tag{6d}$$
$$+\mathbf{K}(t)(z(t+\Delta t) - h(\mathbf{F}(\Delta t)\hat{\mathbf{x}}(t|t))) \tag{6e}$$
$$\mathbf{P}(t+\Delta t|t+\Delta t) = (\mathbf{I} - \mathbf{K}(t)\mathbf{H}(\Delta t))\mathbf{P}(t+\Delta t|t) \tag{6f}$$

where $\mathbf{P}(t)$ is the estimated covariance matrix, which is a $[2m+2]\times[2m+2]$ diagonal matrix with $[0.001, 0.1/1, 0.1/2, ..., 0.1/l, 0.1, 0.2_{1\times m}]$ along the diagonal, $\mathbf{Q}$ is the process noise covariance matrix, which is also a $[2m+2]\times[2m+2]$ diagonal matrix with 0.0001 along the diagonal, σ_R^2 is the observation noise covariance matrix, which is a scalar with a value of 0.01, and $\mathbf{H}(\Delta t)$ is

$$\mathbf{H}^T(\Delta t) = \left(\frac{\partial y}{\partial \mathbf{x}}\right)^T\Bigg|_{\hat{\mathbf{x}}(t+\Delta t|t)=\mathbf{F}\hat{\mathbf{x}}(t|t)} \tag{7a}$$

$$= \begin{bmatrix} 1 \\ \sin\hat{\theta}_1(t+\Delta t|t) \\ \vdots \\ \sin\hat{\theta}_m(t+\Delta|t) \\ \hat{r}_1(t+\Delta t|t)\cos\hat{\theta}_1(t+\Delta t|t) \\ \vdots \\ \hat{r}_m(t+\Delta t|t)\cos\hat{\theta}_m(t+\Delta t|t) \end{bmatrix} \tag{7b}$$

where the $\hat{}$ symbol denotes the estimated value.

To predict future POI positions, the state matrix $\mathbf{x}$ is multiplied j times by the update matrix $\mathbf{F}$ to move j steps ahead:

$$\hat{\mathbf{x}}(t+j\Delta t|t+\Delta t) = \mathbf{F}(\Delta t)^j\hat{\mathbf{x}}(t+\Delta t|t) \tag{8}$$

The predicted position, ${}^I\hat{P}''_{POI}$ is found by calculating (3a) using the predicted $\mathbf{x}(t+j\Delta t|t+\Delta t)$ found above. As the POI's motion is confined to 1D, the direction of the axis of the surgical tool, it is converted to the robot's frame by converting the distance between the POI and the origin (common to both the image and robot frame) from pixels into mm to obtain ${}^R\hat{P}''_{POI}$.

4. Experimental Setup

The experimental setup shown in Fig. 7 uses a 6 MHz 4DL14-5/38 linear 4D transducer connected to a SonixTouch ultrasound scanner (SonixTouch from Ultrasonix, Richmond, BC, Canada) as the image sensor, which has a low frame rate of 34 Hz. The depth of the images was 4.5 cm. The 2D ultrasound images were collected from the ultrasound scanner using a DVI2USB 3.0 frame grabber (Epiphan, Ottawa, ON, Canada). The entire image acquisition, processing delay and upsampling delay is 170 ms. A custom-built mechanical cam (simulated heart) generated the POI motion. The shape of the cam is based on the motion trajectory collected from the movement of a point on the side wall of the heart in a series of clinical ultrasound images of a patient's beating heart. The single degree-of-freedom (DOF) surgical tool (surgical robot) is actuated by a voice coil motor (NCC20-18-020-1X from H2W Technologies Inc., Santa Clarita, CA, USA). To verify the results, real-time position measurements of both the mechanical cam and the robot were collected from two potentiometers (LP-75FP-5K and LP-30FP-1K from Midori America Corp., Fullerton, CA, USA); however the real-time measurement of the mechanical cam's motion was not made available to the controller. The entire system is controlled at a fast sampling rate of 100 Hz.

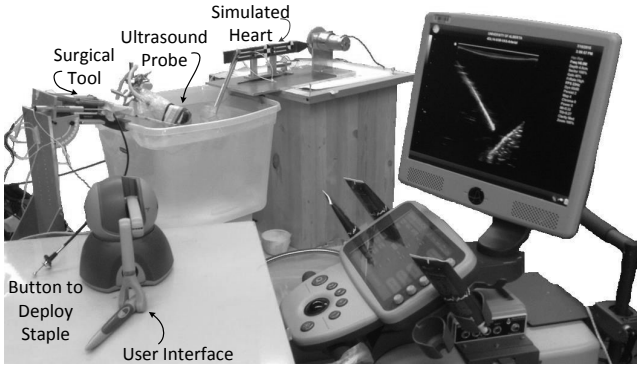

Fig. 7. The experimental setup.

For each trial, the heartbeat motion has a peak-to-peak amplitude of 10 mm and a period of 64 bpm (1.07 Hz). Three error metrics are calculated for each trial: the mean absolute error (MAE) is $\frac{\sum|upsampled-actual|}{l}$, where l is the number of data points in the sample, the integral squared error (ISE) is $\frac{\sum(upsampled-actual)^2}{l}$, and the peak error is

the largest error at a single point in time. The results from each of the trials are summarized in Table 1.

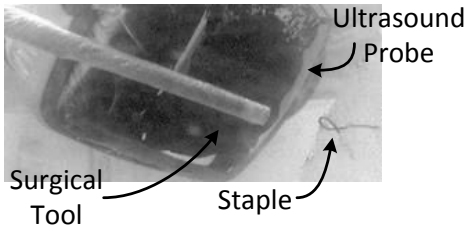

Fig. 8. A staple that has been successfully deployed from the surgical tool into the phantom heart tissue.

4.1. *Surgical Task*

The surgical task presented simulates deploying a staple to secure an annuloplasty ring onto the mitral valve. If the mitral valve is not shaped properly, it may not seal when the ventricle contracts. This allows blood to flow backwards through the heart, making each heart beat less efficient. To correct this, the surgeon enters the heart through the left atrium. The sutures are placed around the mitral valve annulus, the annuloplasty ring is set in place, and the knots are tied. The newly shaped valve is then tested using water before the patients heart is restarted.[26] If securing this annuloplasty ring could be performed while the heart is still beating, the effectiveness of the newly reshaped valve could be evaluated immediately. This user study was approved by the University of Alberta's Research Ethics Office #Pro00055825.

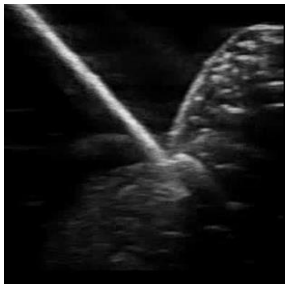

Fig. 9. An example of using excessive force when deploying a staple.

In this study, the participant is asked to deploy the staple into moving heart tissue. The participant moves the surgical tool through teleoperation by moving the stylus of a PHANToM Omni (Geomagic, Cary, NC, USA) – the user interface. The heart tissue is a piece of soft plastic visible under ultrasound. This simulated heart tissue is connected to the mechanical cam and moves in a quasi-periodic fashion – simulated heart. The surgical tool is rigidly attached to a stand and has a 5 cm range of motion. The ultrasound probe is positioned such that the simulated heart's motion and the motion of the surgical tool are visible. The participant views the motion of the simulated heart tissue and the surgical tool on the ultrasound screen. The last element is a button connected to the surgical tool which deploys the staple. An image of a successfully deployed staple is shown in Fig. 8. This task is completed under two conditions: with and without motion compensation. For both conditions, the participants view the ultrasound video of the simulated heart tissue and surgical tool. While completing this task, the participant is told not to press the tool into the tissue such that the tissue deforms.

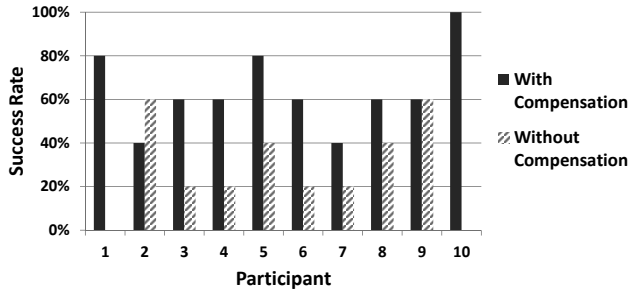

Fig. 10. The rate of successful deployment of the staple for each participant.

Each participant successfully deployed three staples with motion compensation before beginning the trials. They were also allowed to practice under both conditions until they felt comfortable with the system before starting the trials. Each participant completed 10 trials, 5 with motion compensation and 5 without. The trials alternated between the two control conditions starting with motion compensation. If the surgical tool left an indent in the phantom tissue when the staple was deployed (see Fig. 9), the trial was counted as a failure and a penalty was assigned regardless of whether or not the staple deployment was successful.

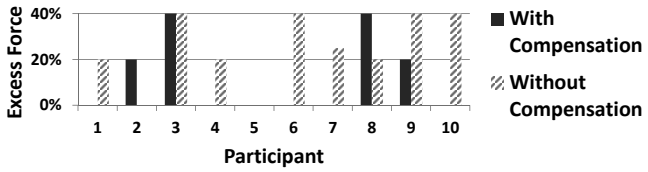

Fig. 11. The rate of the use of excessive force for each participant.

The trials included 10 participants who were not surgeons (2 females and 8 males) ages 21-30. When there was no motion compensation, the staple was successfully deployed in 28% of the trials and excessive force, leaving an indent in the tissue, occurred in 24.5% of the trials. When motion compensation was provided, the success rate more than doubled to 64% and the use of excessive force was reduced by half to 12% of the trials. The success rate of each participant is given in Fig. 10 and the rate of the use of excessive force is given in Fig. 11.

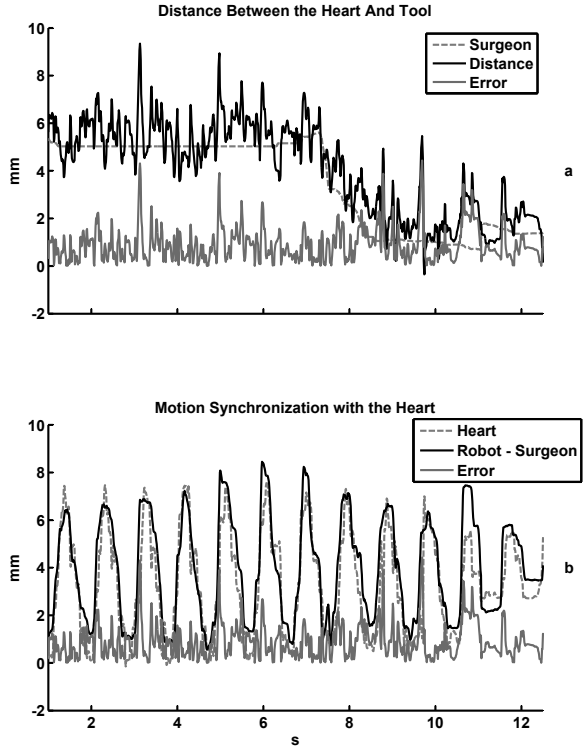

Fig. 12. The result when motion compensation is provided. In case (a), the dashed pink line is the user's motion, the solid black line is the distance between the surgical tool tip and the heart tissue, and the red line is the error between these two. Case (b) shows the motion synchronization. Here, the surgeon's motions have been subtracted from the surgical tool tip's motion leaving the POI following portion of the surgical tool tip's motion – the solid black line. The heart's motion is the dotted pink line and the error between the two is the red line.

To compare the success rates we used a two-tailed *t-test* and obtained the p-value of the null hypothesis $\mu_1 = \mu_2$ for the 10 trials.[27] The probability of the results assuming the null hypothesis for the success of the staple deployment with and without compensation was 0.01 and for the use of excess force with and without compensation was 0.10. These results indicate that there was a significant difference between providing and not providing motion compensation with respect to the successful deployment of the staple, but not with respect to the use of excessive force.

When motion compensation was not provided, only 3 of the 10 participants, participants 3, 9, and 10 attempted to manually compensate for the heart's motion. These participants used excessive force in 40% of the trials, which is much higher than the average rate of 24.5%. The majority of the participants simply waited for the tissue to approach the tool tip and then deployed the staple at the correct time. This method is possible, because the staple can be deployed very quickly. However, the tasks in most surgical procedures cannot be performed so quickly and would hence have higher failure rates as this method would no longer be feasible.

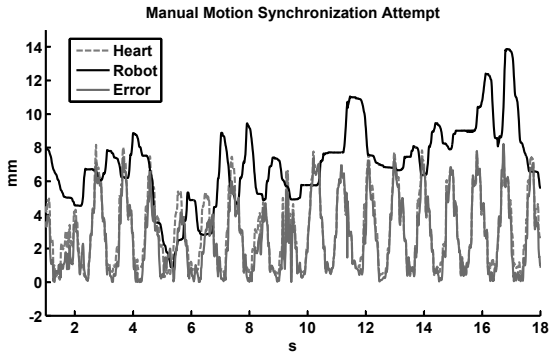

Fig. 13. The result when no motion compensation is provided. Here the user tries to manually compensate for the heart's motion. The surgical tool tip's motion is the solid black line, the heart's motion is the dotted pink line and the error between the two is the red line.

When motion compensation was provided, it was easier for the user to move the surgical tool towards the moving heart tissue. The user's motions for this case creates the pink line in Fig. 12a. The user's motion simply moves the surgical tool tip towards the heart tissue. The solid black line in this figure is the resulting distance between the surgical tool tip and the POI and the solid red line is the error. Part (b) of Fig. 12 shows the result of the motion compensation. Here, the surgeon's motion has been subtracted from the surgical tool tip's motion to remove the offset between the surgical tool tip and the heart tissue – the solid black line. The POI's motion is given by the dashed pink line and the error is given by the solid red line. The MAE tracking error when motion compensation is provided is 0.95 mm, the ISE tracking error is 3.58 mm^2, and the absolute value of the peak tracking error is 3.58 mm. It is much harder for the user to follow the POI's motion when no motion compensation is provided. Fig. 13 shows the surgeon's motion – the solid black line and the POI's motion – the dashed pink line. It is quite obvious that the errors are quite large – the solid red line. The MAE tracking error when motion compensation is not provided is 4.33 mm, the ISE tracking error is 27.19 mm^2, and the absolute value of the peak tracking error is 11.78 mm.

Table 1. The experimental results

Motion Compensation	MAE (mm)	ISE (mm^2)	Peak Error (mm)
Yes	0.95	1.38	3.58
No	4.33	27.19	11.78

5. Conclusion

Performing a surgical procedure on a freely beating heart is extremely difficult, and most surgical procedures are performed with the aid of a mechanical stabilizer or a heart-lung bypass machine. However, these methods have serious side-effects. Alternatively, if the surgical tool could automatically move in synchrony with the POI on the heart and the surgeon's motions are superimposed through teleoperation, the surgeon would be able to operate on seemingly stationary tissue. This paper presents an image processing and control system for ultrasound-guided robot-assisted beating heart surgery for procedures such as mitral valve annuloplasty. As the position of the heart is measured from ultrasound images that are collected at a slow sampling rate, the position trajectory of the POI is first upsampled to 100 Hz. To overcome the time delay caused by ultrasound image acquisition and processing, the POI motion trajectory is predicted ahead to the current time using an EKF. To show the efficacy of this system, user trials simulating deploying a staple for mitral valve annuloplasty were conducted. The results indicate that the improvement in the success rate when motion compensation is provided is statistically significant. The success rate when motion compensation was not provided was aided by the fact that the participant did not need to follow the heart's motion to successfully deploy the staple. Rather, the participant could simply move the surgical tool to the furthest point in the heart's trajectory so the two came into contact once every beat. They then deployed the staple at the correct moment. This method was successful in this case; however, this method would not be successful for more complicated surgical procedures where the surgical tool must remain in contact with the heart for any length of time.

The average and peak tracking error reported in this work, 0.95 mm and 3.58 mm, is similar to those reported in the literature. Sub-millimetre errors were reported when a 500 Hz camera measured the position of the POI and the time delay was limited to one sample time in [12]. The use of pre-recorded data resulted in average errors as low as 0.669 mm and peak errors as large as 4.3 mm in [5]. However, this method is not viable in real-time. The use of motion compensation after the heart is stabilized by a mechanical stabilizer resulted in small errors of 0.4 and 0.8 mm in the x and y directions and a peak error of 2 mm in the y-direction in [1]. However, this method does not let the heart beat freely. Finally, an average and peak error of 0.97 mm and 3.26 mm respectively was reported in [14] where the POI motion was measured from ultrasound images. A similar user task performed with a hand-held motion compensating surgical tool reported a success rate of 74% when motion compensation was provided and only 32% when motion compensation was not provided.[28]

Acknowledgments

This work was supported by the Natural Sciences and Engineering Research Council (NSERC) of Canada RGPIN 03907 and RGPIN 372042, the Canada Foundation for Innovation (CFI) LOF 28241, an Alberta Innovation and Advanced Education Ministry Small Equipment Grant RCP-12-021, and a University of Alberta Startup Grant.

References

[1] T. Ortmaier, M. Groger, D.H. Boehm, V. Falk, and G. Hirzinger, Motion Estimation in Beating Heart Surgery, in *IEEE Trans. on Biomedical Engineering* **52**(10) (2005) pp. 1729–1740.

[2] G.L. Reed, D.E. Singer, E.H. Picard, and R.W. DeSanctis, Stroke Following Coronary-Artery Bypass Surgery. A Case-Control Estimate of the Risk from Carotid Bruits, in *The New England Journal of Medicine* **319**(1988) pp. 1246–1250.

[3] M.F. Newman, J.L. Kirchner, B. Phillips-Bute, V. Gaver, H. Grocott, R H. Jones, D.B. Mark, J.G. Reves, and J. A. Blumenthal, Longitudinal Assessment of Neurocognitive Function after Coronary-Artery Bypass Surgery, in *New England Journal of Medicine* **344**(6) (2001) pp. 395–402.

[4] M.K. Rausch, W. Bothe, J.P.E. Kvitting, J.C. Swanson, D.C. Miller, E. and Kuhl, Mitral Valve Annuloplasty, in*Annals of Biomedical Engineering* **40**(3) (2012) pp. 750–761.

[5] O. Bebek and M.C. Çavuşoğlu, Intelligent Control Algorithms for Robotic-Assisted Beating Heart Surgery, in *IEEE Trans. on Robotics* **23**(3) (2007) pp. 468–480.

[6] E.E. Tuna, T.J. Franke, O. Bebek, A. Shiose, K. Fukamachi, and M. C. Cavusoglu, Heart Motion Prediction Based on Adaptive Estimation Algorithms for Robotic-Assisted Beating Heart Surgery, in *IEEE Trans. on Robotics* **29**(1) (2013) pp. 261–276.

[7] E.E. Tuna, J.H. Karimov, T. Liu, O. Bebek, K. Fukamachi, and M.C. Çavuşoğlu, Towards Active Tracking of Beating Heart Motion in the Presence of Arrhythmia for Robotic Assisted Beating Heart Surgery, in *PLoS ONE*, **9**(7) (2014) pp. e102877.

[8] J. Rotella, Predictive Tracking of Quasi Periodic Signals for Active Relative Motion Cancellation in Robotic Assisted Coronary Artery Bypass Graft Surgery, in *Master Dissertation, Case Western Reserve University* (2005)

[9] T. Horiuchi, E.E. Tuna, K. Masamune, M.C. Çavuşoğlu, Heart motion measurement with three dimensional sonomicrometry and acceleration sensing, in *Proc. IEEE/RSJ Int. Conf. on Intelligent Robots and Systems* (Vilamoura, 2012) pp. 4143-4149.

[10] Y. Nakamura, K. Kishi, and H. Kawakami, Heartbeat synchronization for robotic cardiac surgery, in *Proc. IEEE Int. Conf. on Robotics and Automation*, (Seoul, 2001) pp. 2014–2019.

[11] R. Ginhoux, J.A. Gangloff, M.F. de Mathelin, L. Soler, J. Leroy, and J. Marescaux, Model Predictive Control for Tracking of Repetitive Organ Motions Dur-

ing Teleoperated Laparoscopic Interventions, in *Proc. European Control Conference* (Cambridge, 2003) pp. 2481–2486.

[12] R. Ginhoux, J. Gangloff, M. de Mathelin, L. Soler, M.M.A. Sanchez, and J. Marescaux, Active filtering of physiological motion in robotized surgery using predictive control, in *IEEE Trans. on Robotics* **21**(21) (2005) pp. 67–79.

[13] T.J. Franke, O. Bebek, M.C. Çavuşoğlu, Improved prediction of heart motion using an adaptive filter for robot assisted beating heart surgery, in *Proc. IEEE/RSJ International Conference on Intelligent Robots and Systems*, (San Diego, 2007) pp. 509–515.

[14] S.G. Yuen, P.M. Novotny, and R.D. Howe, Quasiperiodic predictive filtering for robot-assisted beating heart surgery, in *Proc. IEEE Int. Conf. on Robotics and Automation* (Pasadena, 2008) pp. 3875–3880.

[15] D.T. Kettler, R.D. Plowes, P.M. Novotny, N.V. Vasilyev, P.J. del Nido, and R.D. Howe, An active motion compensation instrument for beating heart mitral valve surgery, in *Proc. IEEE/RSJ Int. Conf. on Intelligent Robots and Systems* (San Diego, 2007) pp. 1290–1295.

[16] P. Novotny, Real-time processing of three dimensional ultrasound for intracardiac surgery, in *Ph.D. dissertation, Harvard University* (2007)

[17] P.M. Novotny, J.A. Stoll, P.E. Dupont, and R.D. Howe, Real-Time Visual Servoing of a Robot Using Three-Dimensional Ultrasound, in *Proc. IEEE Int. Conf. on Robotics and Automation* (Roma, 2007) pp. 2655–2660.

[18] A.P.L. Bó, P. Poignet, C. and Geny, Pathological Tremor and Voluntary Motion Modeling and Online Estimation for Active Compensation, in *IEEE Transactions on Neural Systems and Rehabilitation Engineering* **19**(2) (2011) pp. 177–185.

[19] T.M Kowalewski, J. Rosen, L.C. Chang, M.N. Sinanan, and B. Hannaford, Optimization of a Vector Quantization Codebook for Objective Evaluation of Surgical Skill, in *Medicine Meets Virtual Reality 12: Building a Better You: the Next Tools for Medical Education, Diagnosis, and Care* (IOS Press, Amsterdam, 2004), pp. 174–179.

[20] J. Li, M. Tavakoli, V. Mendez, and Q. Huang, Passivity and Absolute Stability Analyses of Trilateral Haptic Collaborative Systems, in *Journal of Intelligent and Robotic Systems* **78**(1) (2015) pp.3–20.

[21] L. Santos, and R. Cortesão, A Dynamically Consistent Hierarchical Control Architecture for Robotic-Assisted Tele-Echography with Motion and Contact Dynamics Driven by a 3D Time-of-Flight Camera and a Force Sensor, in*Proc. IEEE int. Conf. on Robotics and Automation* (Seattle, 2015) In press.

[22] M. Bowthorpe, M. Tavakoli, H. Becher, and R.D. Howe, Smith Predictor Based Robot Control Ultrasound-guided Teleoperated Beating-heart Surgery, in *Proc. IEEE Journal of Biomedical and Health Informatics* **18**(1) (2013) pp.157–166.

[23] M. Bowthorpe, M. Tavakoli, H. Becher, and R.D. Howe, Smith Predictor Based Control in Teleoperated Image-guided Beating-heart Surgery, in *Proc. IEEE Int. Conf. on Robotics and Automation* (Karlsruhe, 2013) pp. 5825–5830.

[24] OpenCV Library: http://opencv.org

[25] P.J. Parker, and B.D.O Anderson, Frequency tracking of nonsinusoidal periodic signals in noise, in *Signal Processing* **20**(2) (1990) pp. 127–152.

[26] F. Maisano, and R. Skantharaja, and P. Denti, and A. Giacomini, and O. Alfieri, Mitral annuloplasty, in *Multimedia Manual of Cardio-Thoracic Surgery* **2009**(0918) (2009).

[27] G.E. Snedecor, W.G. and Cochran, The Two-tailed T-Test, in *Statistical Methods* (The Iowa State University Press Ames, 1967), pp.59–60.

[28] S. Yuen, S. Kesner, N. Vasilyev, P. Del Nido, and R. Howe, 3D Ultrasound-Guided Motion Compensation System for Beating Heart Mitral Valve Repair, in *Medical Image Computing and Computer-Assisted Intervention* **5241** (2008) pp.711–719.

Meaghan Bowthorpe received her B.Sc. degree in Electrical Engineering from the University of Alberta in 2010. She is currently pursuing a Ph.D. in Electrical and Computer Engineering at the University of Alberta and is working on motion tracking algorithms for image-guided robot-assisted surgery.

Mahdi Tavakoli is an Associate Professor in the Department of Electrical and Computer Engineering, University of Alberta, Canada. He received his BSc and MSc degrees in Electrical Engineering from Ferdowsi University and K.N. Toosi University, Iran, in 1996 and 1999, respectively. He received his PhD degree in Electrical and Computer Engineering from the University of Western Ontario, Canada, in 2005. In 2006, he was a postdoctoral researcher at Canadian Surgical Technologies and Advanced Robotics (CSTAR), Canada. In 2007-2008, he was an NSERC Post-Doctoral Fellow at Harvard University, USA. Dr. Tavakoli's research interests broadly involve the areas of robotics and systems control. Specifically, his research focuses on haptics and teleoperation control, med-

ical robotics, and image-guided surgery. Dr. Tavakoli is the lead author of Haptics for Teleoperated Surgical Robotic Systems (World Scientific, 2008).